Neuropeptide oxytocin facilitates its own brain-to-periphery uptake by regulating blood flow dynamics and permeability

Preethi Rajamannar[1,2], Oren Raz[3] and Gil Levkowitz[1,2*]

Departments of [1]Molecular Cell Biology, [2]Molecular Neuroscience, and [3]Physics of Complex Systems, Weizmann Institute of Science, PO Box 26, Rehovot 7610001, Israel

*Correspondence should be addressed to

G.L. gil.levkowitz@weizmann.ac.il

Running title: Oxytocin regulates pituitary blood flow and permeability

Key words: neurohormones, oxytocin, arginine-vasopressin, neurohypophysis, neuroendocrine, zebrafish

Abstract

The hypothalamo-neurohypophyseal system is an important neuroendocrine brain-to-blood conduit through which the neurohormones oxytocin and arginine-vasopressin are released from the brain into the general circulation to affect peripheral physiological functions such as salt balance, metabolism and reproduction. However, the mechanism which executes fast and efficient neurohormone release to the periphery remains unsolved. We show, using live imaging in zebrafish, that a hyperosmotic physiological challenge elicits a local increase in neurohypophyseal blood flow velocities and a change in capillary diameter, which is dictated by the geometry of the hypophyseal vascular microcircuit. Genetic ablation of oxytocin neurons and inhibition of oxytocin receptor signaling attenuated changes in capillary blood flow and diameter. Optogenetic stimulation of oxytocin neurons resulted in an oxytocin receptor-dependent increase in blood flow velocities. Lastly, both osmotic challenge and oxytocin neuronal activation elicited a local rise in neurohypophyseal capillary permeability in an oxytocin signaling-dependent manner. Our study demonstrates that physiologically elicited changes in neurohypophyseal blood flow and permeability are regulated by oxytocin. We propose that oxytocin-dependent neuro-vascular coupling facilitates its efficient uptake into the blood circulation, suggesting a self-perpetuating mechanism of peripheral hormone transfer.

INTRODUCTION

How the brain exerts control over peripheral functions is a fundamental question that has occupied researchers for over a century. In the early 1900s, Berta and Ernest Scharrer noticed that neurons residing in the hypothalamus of a small freshwater fish have properties similar to hormone-secreting endocrine cells (*1, 2*). This discovery served as an inspiration for Scharrers' "neurosecretion concept", arguing that hypothalamic neurons release packets of neuro-hormones from the brain into the general circulation by directly projecting their axons onto local blood vessels of the posterior pituitary gland, also known as the neurohypophysis. This brain-to-periphery neurosecretion machinery termed the hypothalamo-neurohypophyseal system (HNS), is evolutionarily conserved among all vertebrate species and is a major neuroendocrine system responsible for the secretion of the neuro-hormones oxytocin (OXT) and arginine-vasopressin (AVP) from hypothalamic axonal termini onto fenestrated (i.e., permeable) capillary network of the neurohypophysis to affect peripheral organs. In the periphery, AVP regulates water homeostasis by increasing the water permeability of the kidney, whereas OXT regulates labor and milk let-down by causing the contraction of the uterine smooth muscles and the myoepithelial cells of breast ducts, respectively(*3, 4*). In teleost fish species, OXT and AVP are involved in osmoregulation and regulating reproductive success(*5, 6*).

Despite the physiological importance of OXT and AVP, there is a gap in our understanding of their regulated secretion into the blood. The prevailing dogma maintains that in response to physiological demands, hypothalamic OXT and/or AVP neurons are stimulated, released from the axonal termini into the neurohypophysis, taken up by blood capillaries into the systemic circulation, and transported to target tissues (*7*). This process requires tight regulation between the secretory neurons, the release of the hormones, and their transport into the blood. However, it has been noted that a simplified stimulus–secretion coupling mechanism, wherein the release of the contents of vesicles upon neuronal activation (e.g. neurotransmitter release), is directly associated with its effect on the target neuron does not apply in the context of neuroendocrine effect on peripheral targets (*8*). Thus, while the measured firing rhythms of OXT and/or AVP neurons range within milliseconds or even seconds, it takes several minutes to detect them in the peripheral blood (*9*). Moreover, unlike the dense synaptic connection between neurons or the tightly arranged neurovascular units observed in the brain, HNS nerve endings do not form compact, juxtaposed connections with pituitary blood vessels. They rather form numerous

axonal varicosities packed with large dense core vesicles that release their content into the neurohypophysis, wherein the secreted neurohormones are required to transverse the cell-abundant pituitary parenchyma, the endothelial basement membrane, and then enter the endothelial lumen (*10*). ***It is, therefore, highly plausible that an additional driving force is required to facilitate efficient coupling between neurohormone release and its vascular uptake, leading to downstream effects on peripheral target tissues.***

In the brain, synaptic activity increases local blood flow to meet the metabolic needs of a firing neuron, a process termed neurovascular coupling. It has been suggested that endocrine cells of the pituitary gland and pancreas are coordinated with blood vessels to generate hormone pulses (*11, 12*). Thus, local blood flow in neuroendocrine interfaces may facilitate efficient hormone uptake rather than just a means to cope with the increased demands for oxygen.

Here, we hypothesized that in the neurohypophysis, activity-dependent changes in local blood flow modulate peripheral neurohormone uptake. Using live imaging of the zebrafish HNS, we monitored hypophyseal vascular dynamics in unanesthetized animals. We demonstrate that the physiological activation of oxytocin neurons is directly coupled to changes in blood flow velocity and capillary permeability. We further demonstrate that these physiologically elicited vascular changes are regulated by oxytocin, suggesting that oxytocin facilitates its own brain-to-periphery effects.

RESULTS

Physiological osmotic challenge increases local neurohypophyseal blood flow

To study neuro-vascular coupling in the HNS, we have devised a live-imaging platform using the zebrafish model. We have previously established that the development, cell biology, and anatomy of the HNS neurovascular interface are conserved between zebrafish and mammals (*13-15*). The core components of larval zebrafish HNS neurovascular interface comprised of elaborate oxytocinergic axonal varicosities, the hypophyseal artery (HyA), which conveys blood flow into a capillary loop (HyC) and a venous hypophyseal outlet (HyV) (**Fig. 1A**). This relatively simple and discernible anatomical architecture allowed us to reproducibly monitor vascular dynamics in the same locale within multiple unanesthetized zebrafish larvae. To monitor blood flow, we employed the *Tg(l-fabp:DBP-EGFP)* reporter (*16, 17*) (**Fig. 1B,C**),

97 in which a serum albumin-like molecule is labeled, allowing visualization and quantification
98 of flow velocities calculated from displacement time kymographs of red blood cells (RBC)
99 (**Fig. S1B**). Capillary diameter was monitored using an endothelial-specific transgenic
100 *Tg(kdrl:EGFP)* reporter (**Fig. S1C**).

101 To examine whether physiological activation of the HNS altered hypophyseal blood flow,
102 we employed a hyperosmotic challenge known to stimulate OXT and AVP neurons (*18, 19*)
103 (**Fig. S1A**). When zebrafish larvae were acutely transferred from freshwater to hyperosmotic
104 solution equivalent to 50% seawater (17.5 ppt), we observed significant activation of OXT
105 neurons, displaying increased *c-fos* expression in their soma (**Fig. 1D,E**). This hyperosmotic
106 challenge induced a robust increase in blood flow (**Fig. 1F,G**) and variability of RBCs
107 velocities (**Fig. 1H**). The single-sided amplitude spectra, as computed by a Fast Fourier
108 transformation (FFT), indicated that the osmotic challenge induced an increase in the amplitude
109 of velocity fluctuations below 2Hz (**Fig. 1I**).

110 To ensure that the effect of osmotic challenge on blood flow was specific to the hypophyseal
111 capillary, we measured blood flow in the anterior mesencephalic central artery (AMCtA),
112 which is a well-discernable vascular brain structure located at a similar depth and of similar
113 diameter as the hypophyseal capillary loop (**Fig. 1A**). We found that osmotic challenge did not
114 affect the measured flow parameters of AMCtA vessel (**Fig. 1J-M**).

115 These results show that a physiological challenge, which activates OXT neurons elicits a
116 specific local increase in hypophyseal blood flow velocity.

117

118 **The relationship between flow velocity and diameter is determined by HNS vascular**
119 **geometry**

120 According to Poiseuille's law for viscous fluids, it was expected that local vasoconstriction
121 of a single capillary would increase flow resistance, resulting in decreased blood flow velocity
122 (*20*). However, we observed that the osmotic challenge, which caused an increase in velocity
123 was accompanied by a decrease in hypophyseal capillary diameter (**Fig. 2A-C**). This effect was
124 specific as the diameter of the adjacent AMCtA capillary did not change following the osmotic
125 challenge (**Fig. 2D-F**). Since it was shown that the geometry of the microvasculature network
126 in the brain plays a crucial role in determining blood flow behaviour (*21, 22*), we resolved the

127 relationship between blood flow velocity and capillary diameter considering the structure of
128 the zebrafish hypophyseal vascular microcircuit. This structure is comprised of a stereotypic
129 arterial inlet, capillary loop, and venous outlet; each having its corresponding length (L), and
130 radius (r) (**Fig. 2G**). We expressed the capillary velocity (V_2) in terms of the vascular
131 components' radii and lengths, according to Poiseuille's law, considering a range of relevant
132 inlet-outlet total pressure differences (Δp) (**Fig. 2G and S1E,** for details, see '*Methods*'
133 section). Plotting the resolved V_2 values as a function of capillary radii revealed that flow
134 velocity is inversely proportional to an increase in capillary radii that are larger than 3 microns
135 (**Fig. 2H**). This inverse proportionality between capillary velocity and diameter, aligned with
136 our measured values of the hypophyseal capillary radii (3-6 μm **Fig. 2B**). Thus, in accordance
137 with our velocity and radii measurements, we found that for basal velocity to increase after
138 osmotic challenge within a range of relevant estimated inlet-outlet pressure differences (Δp),
139 there must be either a small decrease in radii with a small increase in Δp or a large decrease in
140 radii with no change in Δp (**Fig. 2H'**).

141 These results show that an increase in blood flow velocity can be caused by vasoconstriction
142 given the geometry of the hypophyseal vascular microcircuit.

143

144 **Hypophyseal blood flow is regulated by oxytocin signaling**

145 We tested whether the observed neuronal and vascular responses to an osmotic challenge
146 are coupled. This was demonstrated using the *Tg(oxt:Gal4;UAS:NTR-mCherry)* genetic
147 system for conditional cell ablation (**Fig. 3A**). Specific death of OXT cells expressing the
148 nitroreductase (NTR) enzyme was induced by the administration of the drug Nifurpirinol
149 (NFP), which is converted to a cytotoxic agent by NTR (*23-25*). Treatment of these transgenic
150 animals for 18 hours with NFP led to a significant decrease in OXT-positive hypophyseal
151 axonal projections (**Fig. 3B,C**). When subjected to an osmotic challenge, control Gal4/UAS-
152 negative larvae displayed increased blood flow velocity while their sibling larvae with ablated
153 OXT neurons did not (**Fig. 3D,E**). The mean capillary blood flow velocity, amplitudes, and
154 frequency spectra, and variability in velocity did not show a significant difference after the
155 osmotic challenge of OXT ablated larvae (**Fig. 3F-I**). Notably, whereas the osmotic challenge
156 caused vasoconstriction in non-ablated controls, it led to vasodilation of hypophyseal
157 capillaries in larvae with ablated OXT neurons, presumably as a response to the absence of

158 OXT neurovascular innervation and low basal OXT secretion (**Fig. 3J-M**). The effects of this
159 genetic OXT-ergic ablation were confined to the hypophyseal vasculature as they were not
160 observed in the control AMCtA vessel (**Fig. 3N-P**).

161 In view of our observed effects of OXT neuron ablation, we hypothesized that OXT itself
162 might regulate local hypophyseal blood flow velocity upon its release. We found that
163 endothelial cells isolated from zebrafish pituitaries express mRNAs encoding the two known
164 functional OXT receptors, *oxtra,* and *oxtrb,* with markedly higher expression levels of *oxtrb*
165 (**Fig. S2**). We therefore examined whether the administration of a selective oxytocin receptor
166 antagonist, L-368,899, which is known to inhibit both zebrafish OXT receptors (*26, 27*), affects
167 hypophyseal blood flow. We found that larvae treated with L-368, 899, were refractory to the
168 osmotic challenge in terms of challenge-induced changes in mean flow velocity parameters
169 (**Fig. 4A-F**) and capillary diameter (**Fig. 4G-J**). Administration of L-368, 899 did not influence
170 blood flow velocity in the extra-hypophyseal AMCtA blood vessel ruling out a general
171 systemic effect of the antagonist (**Fig. 4K-M**).

172 Next, we tested whether direct activation of OXT neurons, rather than through osmotic
173 challenge, is sufficient to modulate hypophyseal blood flow and diameter. To stimulate OXT
174 neurons, we employed the CoChR-tdTomato channelrhodopsin variant, an efficient
175 optogenetic tool for zebrafish (*28*). Injection of *UAS:CoChR-tdTomato* construct into the OXT
176 specific driver line, *Tg(oxt:Gal4)* (*29*), resulted in specific expression of the CoChR-tdTomato
177 protein in OXT neurons (**Fig. 5A,B**). Exposure of *Tg(oxt:Gal4;UAS:CoChR-tdTomato)* larvae
178 to blue light resulted in a transient but significant increase in blood flow velocity, which peaked
179 at approximately 30-50 seconds following light exposure (**Fig. 5D, E**). The control CoChR-
180 tdTomato-negative siblings did not respond to blue light (**Fig. 5C, E**). Light-activated CoChR-
181 positive larvae exhibited a marked increase in $\Delta V/V_0$ as compared to their CoChR-negative
182 siblings (**Fig. 5F**). The responses of hypophyseal vasculature to optogenetic stimulation of
183 OXT neurons were dependent on oxytocin receptor signalling as the above effects were
184 significantly attenuated by the administration of the OXT receptor antagonist, L-368, 899 (**Fig.
185 5G-I**). In accordance with the vasoconstrictive response of the hypophyseal capillary to
186 osmotic challenge, light activation of CoChR-positive, but not CoChR-negative, OXT neurons
187 caused a reduction in mean capillary diameter across time (**Fig. 5J-M**). As in the case of the
188 increased flow velocity, CoChR-induced vasoconstrictive response was inhibited by L-368,
189 899 (**Fig. 5N-P**). Notably, hypophyseal vascular responses (i.e., flow and diameter) to

190 optogenetic activation of OXT neurons were transient as compared to the hyperosmotic
191 challenge. Although this may imply the existence of additional mediators of the effects of
192 osmotic challenge on hypophyseal vascular dynamics, it could be due to the artificial activation
193 of OXT neurons through optogenetics, as opposed to a genuine physiological stimulus, which
194 activates these neurons.

195 These results show that local hypophyseal vascular responses triggered by a hyperosmotic
196 physiological challenge are coupled to OXT neuronal activation and are mediated by OXT
197 receptor(s).

198

199 **Hypophyseal vascular permeability is regulated by OXT signaling**

200 We hypothesized that OXT-mediated neurovascular-coupling may affect the vascular
201 passage of neurohormones and other proteins by regulating diffusion rate through the
202 fenestrated hypophyseal capillaries (*16*). We visualized and quantified hypophyseal capillary
203 permeability using the *Tg(l-fabp:DBP-EGFP)* reporter described above (**Fig. 6A**). We
204 performed fluorescent recovery after photo-bleaching (FRAP) followed by line scan imaging
205 comparing the fluorescent recovery of bleached and unbleached regions of interest positioned
206 on either side of the hypophyseal capillary (**Fig.6A', B**). Paired comparisons of permeability
207 before and after the challenge indicated that the average time taken to recover half the initial
208 fluorescent intensity ($T_{1/2}$) following an osmotic challenge was significantly shorter than in the
209 basal condition, indicating a higher rate of diffusion through the hypophyseal capillary (**Fig.**
210 **6C**).

211 We then investigated the inter-dependent relationship between blood flow velocity and
212 permeability. We have previously shown that Tgf-β signaling regulates hypophyseal vascular
213 permeability (*13*). We now show that albeit the observed attenuation of basal hypophyseal
214 permeability by the selective TGF-β receptor inhibitor, SB431542 (**Fig. 6D, E**), blocking Tgf-
215 β signaling did not affect either the basal blood flow velocity or the response to osmotic
216 challenge (**Fig. 6F**). We next examined whether decreasing blood flow affects permeability.
217 We observed that treatment of zebrafish larvae with the cholinergic receptor inhibitor alpha-
218 bungarotoxin (α-BTX) for 150 seconds led to a nearly 50% reduction in blood flow velocity
219 (**Fig. 6G-H**). This reduction in blood flow had no effect on hypophyseal vessel permeability
220 (**Fig. 6I**).

221 These results indicate that hypophyseal vascular permeability and blood flow velocity are
222 mutually independent.

223 To determine the involvement of OXT signaling in hypophyseal vascular permeability, we
224 performed the FRAP analysis in the presence of the OXT receptor antagonist. Basal
225 permeability was measured continuously at different time points following the administration
226 of the OXT receptor antagonist. A significant increase in $T_{1/2}$ was observed up to an hour after
227 the administration of the antagonist, indicating a cumulative decrease in protein diffusion rate
228 through the hypophyseal capillary (**Fig. 6J**). Furthermore, the permeability-enhancing effect
229 of OC was also attenuated in antagonist-treated larvae as compared to their untreated siblings
230 (**Fig. 6K**).

231 The involvement of OXT in modulating permeability was further determined by direct
232 optogenetic activation of OXT neurons combined with FRAP analysis. A significant decrease
233 in $T_{1/2}$ was measured in light-activated, CoChR-tdTomato-expressing larvae compared to their
234 inactivated basal state (**Fig. 6L**). The control CoChR-negative larvae showed no response to
235 light (**Fig. 6L**). Thus, direct activation of oxytocin neurons enhances hypophyseal
236 permeability.

237 Taken together, our data show that hyperosmotic physiological challenge elicits an increase
238 in local blood flow velocity and permeability of the hypophyseal vasculature, where OXT is
239 released into the peripheral circulation. These hypophyseal vascular responses are influenced
240 by the local vascular geometry and are coupled to OXT neuronal activation, which is mediated
241 by OXT receptors. We submit that OXT may function as a self-perpetuating hormone that
242 facilitates its own peripheral uptake by regulating blood flow dynamics.

243

244 **DISCUSSION**

245 Neurohormones are key factors interfacing between the brain and periphery, yet not much
246 is known about their behavior at the site of release, and in particular, the factors affecting their
247 uptake into the blood. We focus here on the evolutionarily conserved HNS, which is a canonical
248 neuroendocrine interface wherein neurohormones are directly released from the brain into the
249 blood. The data we have gathered indicates that when faced with a hyperosmotic physiological
250 challenge, there's a noticeable increase in hypophyseal blood flow velocity and vascular

permeability where OXT is released into the peripheral circulation. The local hypophyseal vascular responses to OXT neuronal activation are influenced by vascular geometry and mediated by OXT receptors. This leads us to propose that OXT may function as a self-perpetuating hormone, regulating its own peripheral uptake by influencing blood flow dynamics and permeability.

Neurovascular coupling in the HNS

Upon stimulation of OXT neurons, OXT is released from the nerve termini into the hypophyseal perivascular space and thereafter exerts effects on peripheral target tissues. However, there is a gap in our understanding of the exact events that bring about efficient transport of OXT to the periphery. Unlike the rapid, short-distanced post-synaptic actions of neurotransmitters in the brain, OXT must travel a long distance through the dense hypophyseal perivascular space and its concentration in the blood must increase rapidly in response to physiological demands. This suggests that additional factors may be required for an efficient coordination between the release of neurohormones and their peripheral effects. We hypothesized that activity-mediated axonal release needs to be coupled to blood flow to regulate an effective transfer of OXT into the systemic circulation. However, despite extensive understanding of the electrical activity of oxytocin (OXT) neurons, the role of local blood flow in coordinating neurohormone secretion remains unclear (*30, 31*). Lafont et al. inferred the existence of such a mechanism, demonstrating that the injection of growth hormone-releasing hormone (GHRH) leads to increased local blood flow, coinciding with the timing of the growth hormone (GH) pulse in the peripheral circulation (*32*). These authors discussed the possibility that flow dynamics of the pituitary microvasculature network may influence the pulsatile secretion of growth hormone (*32*).

We show here that an osmotic challenge stimulates OXT neuronal activity concomitant with a specific local increase in volumetric blood flow in the hypophyseal capillary abutting OXT axons termini. This result is in agreement with the reported increased neurohypophyseal blood flow in chronically water-deprived rats (*33, 34*). Others have recently shown a connection between osmotic challenge and changes in supraoptic nucleus (SON) blood flow (*35*). They reported that an acute systemic salt load activates AVP neurons, decreasing blood flow and causing temporary hypoxia, which intensifies the excitatory response of AVP neurons to the systemic hyperosmotic salt challenge (*35*).

282 Local regulation of organ perfusion rate relies on local changes in vascular resistance, which
283 is controlled by capillary radius (*36, 37*). Thus, local vasoconstriction of a single capillary,
284 obeying Poiseuille's flow, will increase resistance and decrease flow (*20*). Having said that, the
285 geometry of a particular microvasculature network, including factors such as capillary length,
286 branching patterns and positions of inlet-outlet, plays an important role in determining flow
287 velocity (*22, 38*). In the case of the specific configuration of the hypophyseal vascular circuit,
288 we found that blood flow velocity increases upon vasoconstriction. This result also fits our
289 theoretically resolved relationship between blood flow velocity and capillary diameter,
290 considering the specific architecture, lengths, and radii of the hypophyseal vascular
291 components.

292

293 **Role of oxytocin signaling**

294 Vascular endothelial cells were shown to express the OXT receptor and have been
295 implicated in the regulation of vascular tone and blood pressure in mammals and fish (*39-43*).
296 It was shown that OXT can exert both vasodilation and vasoconstriction via differential
297 activation of either endothelial nitric oxide or ERK signaling (*39*). We show here that, as in
298 other species, zebrafish OXT neurons are osmoresponsive, and the effect of osmotic challenge
299 on hypophyseal blood flow is mediated by OXT signaling. Similarly, increased osmolality,
300 which was induced by dehydration, led to an increased blood flow in the rat neurohypophysis
301 (*33, 34*). Using Brattleboro rats, Kapitola et al. concluded that the increase in hypophyseal
302 blood flow following dehydration could not be mediated by AVP as these rats cannot
303 synthesize this neurohormone (*34*). However, it is likely that OXT is accountable for the
304 observed dehydration effect on Brattleboro rat hypophysis. This is supported by our findings
305 that the impact of hyperosmotic challenge is mediated by OXT signaling, and that direct
306 optogenetic stimulation of OXT neurons influences both blood flow and diameter.

307 We show that endothelial cells express OXT receptors and that blocking OXT signaling
308 attenuates the induced changes in blood flow and capillary diameter. However, it is important
309 to note that other cell types in the neurohypophysis may also play a role in OXT-mediated
310 vascular response. For example, pericytes have been implicated in the regulation of blood flow
311 in the brain (*44-46*). Additionally, hypophyseal astroglial pituicytes, which receive synaptoid

connections from HNS axon termini, facilitate the release of OXT and AVP to the periphery in response to parturition, lactation, and dehydration (*29, 47, 48*).

Hypophyseal vascular permeability

Although the HNS is considered part of the central nervous system, its vascular component has unique properties that differ from neurovascular units in other brain areas. Unlike most BBB-containing vessels of the CNS, neurohypophyseal capillaries are fenestrated, allowing bi-directional transfer of HNS hormones and blood-borne substances between the brain and circulation (*13, 16, 49*). Our research shows that protein diffusion through the hypophyseal capillary increases after a hyperosmotic challenge. Although we show that the increase in hypophyseal blood flow velocity and permeability appears to be independent of one other, both occur in an oxytocin-dependent manner. Thus, blocking OXT signaling decreases hypophyseal permeability and direct activation of OXT neurons enhances permeability.

Modulation of local blood flow has been linked to hormonal uptake in several instances. For example, somatostatin causes vasoconstriction, reducing blood flow and increasing vascular permeability of pial vessels of the parietal cortex (*50*). Blood flow in the median eminence, which contains fenestrated capillaries, influences food intake by regulating the access of ghrelin to the arcuate nucleus (*51, 52*). Finally, pericytes, which regulate blood flow (*45, 46*) were shown to regulate vascular permeability to circulating leptin (*53*). We propose that in the case of the neurohypophysis, oxytocin orchestrates an efficient neuroendocrine secretion machinery by affecting both hypophyseal blood flow velocity and permeability, thereby coupling its own release and transport into the blood.

Stimulus-secretion-uptake coupling

Based on the results we have presented, we propose the following paradigm, which we term '*stimulus-secretion-uptake coupling*': When HNS neurons are stimulated, OXT is released into the hypophyseal parenchyma and establishes a concentration gradient of OXT between the parenchyma and the local capillary. The diffusion of OXT into the capillary tends to bring the system closer to equilibrium, thus reducing the diffusion of oxytocin into the vessel. The increase in local volumetric flow, which is induced by OXT, has a dual function: **1**) enhancing local transport of OXT to the periphery and **2**) increasing diffusion of the secreted OXT into

342 the blood by maintaining a local oxytocin concentration gradient. This, together with the
343 increased permeability, which is also evoked by OXT, ensures its efficient transfer into the
344 peripheral circulation in response to physiological demands.

345

346 **REFERENCES**

347 1. E. Scharrer, Die lichtempfindlichkeit blinder elritzen.(Untersuchungen über das
348 zwischenhirn der fische I.). *Zeitschrift für vergleichende Physiologie*, (1928).
349 2. E. Scharrer, B. Scharrer, Neurosecretion. *Physiological Reviews* **25**, 171-181 (1945).
350 3. C. A. Pearson, M. Placzek, Development of the medial hypothalamus: forming a
351 functional hypothalamic-neurohypophyseal interface. *Curr Top Dev Biol* **106**, 49-88
352 (2013).
353 4. E. Wircer, S. Ben-Dor, G. Levkowitz, in *Molecular neuroendocrinology : from*
354 *genome to physiology,* D. G. Murphy, Harold, Ed. (John Wiley & Sons, Ltd,
355 Chichester, West Sussex, UK ; Hoboken, NJ, USA, 2016), pp. xiii, 467 pages.
356 5. J. Biran, J. Blechman, E. Wircer, G. Levkowitz, in *Model Animals in*
357 *Neuroendocrinology: From Worm to Mouse to Man,* M. Ludwig, G. Levkowitz, Eds.
358 (Wiley-Blackwell, 2018), pp. 101-103.
359 6. P. Rajamannar, I. Arokiadhas, G. Levkowitz, J. Biran, in *Neuroanatomy of*
360 *Neuroendocrine Systems,* V. Grinevich, Á. Dobolyi, Eds. (Springer International
361 Publishing, Cham, 2021), pp. 95-118.
362 7. G. Leng, M. Ludwig, Neurotransmitters and peptides: whispered secrets and public
363 announcements. *J Physiol* **586**, 5625-5632 (2008).
364 8. P. Le Tissier *et al.*, An updated view of hypothalamic-vascular-pituitary unit function
365 and plasticity. *Nat Rev Endocrinol* **13**, 257-267 (2017).
366 9. G. Leng, N. Sabatier, Measuring Oxytocin and Vasopressin: Bioassays,
367 Immunoassays and Random Numbers. *J Neuroendocrinol* **28**, (2016).
368 10. G. I. Hatton, Pituicytes, glia and control of terminal secretion. *The Journal of*
369 *experimental biology* **139**, 67-79 (1988).
370 11. M. Schaeffer, D. J. Hodson, C. Lafont, P. Mollard, Endocrine cells and blood vessels
371 work in tandem to generate hormone pulses. *J Mol Endocrinol* **47**, R59-66 (2011).

12. M. Schaeffer, D. J. Hodson, C. Lafont, P. Mollard, Functional importance of blood flow dynamics and partial oxygen pressure in the anterior pituitary. *Eur J Neurosci* **32**, 2087-2095 (2010).
13. S. Anbalagan *et al.*, Pituicyte Cues Regulate the Development of Permeable Neuro-Vascular Interfaces. *Dev Cell* **47**, 711-726 e715 (2018).
14. A. Gutnick *et al.*, The hypothalamic neuropeptide oxytocin is required for formation of the neurovascular interface of the pituitary. *Dev. Cell* **21**, 642-654 (2011).
15. Q. Chen *et al.*, Neural plate progenitors give rise to both anterior and posterior pituitary cells. *Dev Cell* **58**, 2652-2665 e2656 (2023).
16. L. Gordon *et al.*, The fenestrae-associated protein Plvap regulates the rate of blood-borne protein passage into the hypophysis. *Development* **146**, (2019).
17. J. Xie, E. Farage, M. Sugimoto, B. Anand-Apte, A novel transgenic zebrafish model for blood-brain and blood-retinal barrier development. *BMC developmental biology* **10**, 76 (2010).
18. G. Leng, J. A. Russell, The osmoresponsiveness of oxytocin and vasopressin neurones: Mechanisms, allostasis and evolution. *J Neuroendocrinol* **31**, e12662 (2019).
19. I. Neumann, R. Landgraf, L. Bauce, Q. J. Pittman, Osmotic responsiveness and cross talk involving oxytocin, but not vasopressin or amino acids, between the supraoptic nuclei in virgin and lactating rats. *J Neurosci* **15**, 3408-3417 (1995).
20. S. P. Sutera, R. Skalak, The History of Poiseuille's Law. *Annual Review of Fluid Mechanics* **25**, 1-20 (1993).
21. P. Blinder *et al.*, The cortical angiome: an interconnected vascular network with noncolumnar patterns of blood flow. *Nat Neurosci* **16**, 889-897 (2013).
22. X. Ji *et al.*, Brain microvasculature has a common topology with local differences in geometry that match metabolic load. *Neuron* **109**, 1168-1187 e1113 (2021).
23. S. Curado, D. Y. Stainier, R. M. Anderson, Nitroreductase-mediated cell/tissue ablation in zebrafish: a spatially and temporally controlled ablation method with applications in developmental and regeneration studies. *Nat Protoc* **3**, 948-954 (2008).
24. D. Bergemann *et al.*, Nifurpirinol: A more potent and reliable substrate compared to metronidazole for nitroreductase-mediated cell ablations. *Wound Repair Regen* **26**, 238-244 (2018).

25. A. R. Nunes *et al.*, Developmental Effects of Oxytocin Neurons on Social Affiliation and Processing of Social Information. *J Neurosci* **41**, 8742-8760 (2021).
26. F. F. Zimmermann, K. V. Gaspary, A. M. Siebel, C. D. Bonan, Oxytocin reversed MK-801-induced social interaction and aggression deficits in zebrafish. *Behavioural Brain Research* **311**, 368-374 (2016).
27. J. Landin *et al.*, Oxytocin Receptors Regulate Social Preference in Zebrafish. *Sci Rep* **10**, 5435 (2020).
28. P. Antinucci *et al.*, A calibrated optogenetic toolbox of stable zebrafish opsin lines. *Elife* **9**, (2020).
29. S. Anbalagan *et al.*, Robo2 regulates synaptic oxytocin content by affecting actin dynamics. *Elife* **8**, (2019).
30. J. A. Russell, G. Leng, A. J. Douglas, The magnocellular oxytocin system, the fount of maternity: adaptations in pregnancy. *Front Neuroendocrinol* **24**, 27-61 (2003).
31. D. A. Poulain, J. B. Wakerley, Electrophysiology of hypothalamic magnocellular neurones secreting oxytocin and vasopressin. *Neuroscience* **7**, 773-808 (1982).
32. C. Lafont *et al.*, Cellular in vivo imaging reveals coordinated regulation of pituitary microcirculation and GH cell network function. *Proc Natl Acad Sci U S A* **107**, 4465-4470 (2010).
33. B. Lichardus, I. Albrecht, J. Ponec, L. Linhart, Water deprivation for 24 hours increases selectively blood flow in posterior pituitary of conscious rats. *Endocrinol Exp* **11**, 99-104 (1977).
34. J. Kapitola, H. Dlouha, J. Krecek, J. Zicha, The effect of dehydration on the neurohypophyseal blood flow in rats with hereditary diabetes insipidus. *Experientia* **33**, 1615-1616 (1977).
35. R. K. Roy *et al.*, Inverse neurovascular coupling contributes to positive feedback excitation of vasopressin neurons during a systemic homeostatic challenge. *Cell Rep* **37**, 109925 (2021).
36. A. R. Pries *et al.*, Resistance to blood flow in microvessels in vivo. *Circ Res* **75**, 904-915 (1994).
37. R. E. Shipley, D. E. Gregg, THE EFFECT OF EXTERNAL CONSTRICTION OF A BLOOD VESSEL ON BLOOD FLOW. *American Journal of Physiology-Legacy Content* **141**, 289-296 (1944).

38. P. Blinder, A. Y. Shih, C. Rafie, D. Kleinfeld, Topological basis for the robust distribution of blood to rodent neocortex. *Proc Natl Acad Sci U S A* **107**, 12670-12675 (2010).
39. Q. Xu *et al.*, Oxytocin-induced endothelial nitric oxide dependent vasorelaxation and ERK1/2-mediated vasoconstriction in the rat aorta. *Korean J Physiol Pharmacol* **26**, 255-262 (2022).
40. N. Japundzic-Zigon, M. Lozic, O. Sarenac, D. Murphy, Vasopressin & Oxytocin in Control of the Cardiovascular System: An Updated Review. *Curr Neuropharmacol* **18**, 14-33 (2020).
41. M. Petersson, T. Lundeberg, K. Uvnas-Moberg, Oxytocin decreases blood pressure in male but not in female spontaneously hypertensive rats. *J Auton Nerv Syst* **66**, 15-18 (1997).
42. M. Jankowski, T. L. Broderick, J. Gutkowska, The Role of Oxytocin in Cardiovascular Protection. *Front Psychol* **11**, 2139 (2020).
43. L. Haraldsen, V. Soderstrom-Lauritzsen, G. E. Nilsson, Oxytocin stimulates cerebral blood flow in rainbow trout (Oncorhynchus mykiss) through a nitric oxide dependent mechanism. *Brain Res* **929**, 10-14 (2002).
44. C. M. Peppiatt, C. Howarth, P. Mobbs, D. Attwell, Bidirectional control of CNS capillary diameter by pericytes. *Nature* **443**, 700-704 (2006).
45. C. N. Hall *et al.*, Capillary pericytes regulate cerebral blood flow in health and disease. *Nature* **508**, 55-60 (2014).
46. D. A. Hartmann *et al.*, Brain capillary pericytes exert a substantial but slow influence on blood flow. *Nat Neurosci* **24**, 633-645 (2021).
47. L. Rosso, J. M. Mienville, Pituicyte modulation of neurohormone output. *Glia* **57**, 235-243 (2009).
48. J. G. Tasker, S. H. Oliet, J. S. Bains, C. H. Brown, J. E. Stern, Glial regulation of neuronal function: from synapse to systems physiology. *J Neuroendocrinol* **24**, 566-576 (2012).
49. S. Miyata, New aspects in fenestrated capillary and tissue dynamics in the sensory circumventricular organs of adult brains. *Front Neurosci* **9**, 390 (2015).
50. J. B. Long, D. D. Rigamonti, K. Dosaka, J. M. Kraimer, A. Martinez-Arizala, Somatostatin causes vasoconstriction, reduces blood flow and increases vascular permeability in the rat central nervous system. *J Pharmacol Exp Ther* **260**, 1425-1432 (1992).

51. N. Romano *et al.*, Median eminence blood flow influences food intake by regulating ghrelin access to the metabolic brain. *JCI Insight* **8**, (2023).
52. M. Schaeffer *et al.*, Rapid sensing of circulating ghrelin by hypothalamic appetite-modifying neurons. *Proc. Natl. Acad. Sci. USA* **110**, 1512-1517 (2013).
53. L. I. Butiaeva *et al.*, Leptin receptor-expressing pericytes mediate access of hypothalamic feeding centers to circulating leptin. *Cell Metab* **33**, 1433-1448 e1435 (2021).
54. G. K. Batchelor, in *An introduction to fluid dynamics*. (Cambridge University Press, 2000), chap. 4.

ACKNOWLEDGEMENTS

We thank Takashi Kawashima and Pablo Blinder for valuable discussions and advice; Roy Hofi, Estar Regev and fish facility personnel. G.L. lab is supported by the Israel Science Foundation (#349/21); Hedda, Alberto, and David Milman Baron Center for Research on the Development of Neural Networks; Wolfe Family Center for Research on Neuroimmunology and Neuromodulation; Sagol Center for Research on the Aging Brain; and Maurice and Vivienne Wohl Biology Endowment and Foundation for Higher Education and Culture. P.R. was supported by a research grant for a student fellowship from the Benoziyo Endowment Fund for the Advancement of Science and by the Weizmann–CNRS Collaboration Program. G.L. is an incumbent of the Elias Sourasky Professorial Chair.

AUTHOR CONTRIBUTIONS

Conceptualization, P.R. and G.L.; Methodology, P.R. Investigation, P.R., O.R. and G.L.; Resources, P.R., Formal analysis, P.R. and O.R.; Writing-original draft, P.R. and G.L.; Writing-review and editing, P.R., G.L., and O.R.; Visualization, P.R.; Funding acquisition, G.L.; Project administration, P.R. and G.L.

MATERIALS AND METHODS

Husbandry and housing conditions of experimental animals

All experiments using zebrafish were approved by the Weizmann Institute's Institutional Animal Care and Use Committee (Application number 00590123-3 and 16970919-3). Zebrafish were maintained and bred using standard protocols and according to FELASA guidelines.

Transgenic animals

The following transgenes were used in this study: *Tg(l-fabp:DBP-eGFP)*,*Tg(kdrl:eGFP), Tg(oxt:gal4-VP16; UAS:NTR-mCherry; l-fabp:DBP-eGFP/kdrl:eGFP), Tg(oxt:gal4-VP16; UAS:CoChR-tdTomato; l-fabp:DBP-eGFP/kdrl:eGFP).* Larvae that were to be imaged were kept in the Danieau's buffer with 0.003% PTU from 24hpf till the day of the experiment.

Organism/ Recombinant DNA	**Allele number**	**ZFIN ID**
Tg(kdrl:eGFP)	s843	ZDB-ALT-050916-14
Tg(l-fabp:DBP-EGFP)	lri500	ZDB-ALT-120118-1
Tg(oxt:Gal4; cmlc2:EGFP)	wz06	ZDB-ALT-171113-2
Tg(UAS:NTR-mCherry)	jh17	ZDB-ALT-110222-4
Tg(UAS:CoChR-tdTomato)	u332	ZDB-TGCONSTRCT-190226-2

In-vivo imaging of live zebrafish

Six days post fertilization (dpf) zebrafish larvae were immobilized with a 30s incubation with 1mg/ml alpha-bungarotoxin followed by a quick wash in E3 media and mounted in 0.8% low-melt agarose in a custom moulded 3cm plate filled with 2% agarose. The plate was filled with 3ml E3 media prior to imaging. Samples were excited using the Zeiss LSM7 Multi-Photon Microscope with a pulsed laser (Coherent Chameleon) tuned to 870nm set at a 4-6% laser intensity (max. 210mW) through a 20x water immersion Pln Apochromatic Lens. Emitted light was detected through the BiG detector after passage through a BP500-550 filter. Line scans were obtained by manually defining a single-pixel scan path (pixel scaling of 0.03um) as required which was then scanned for a pre-defined number of frames using the Galvanometric scanning head.

520 **Osmotic challenge, cell ablation and pharmacological treatments**

521 Zebrafish were osmotically challenged using 50% instant ocean salt (17.5 gr/l; Instant Ocean
522 Sea Salt, Aquarium Systems) dissolved in E3 media (5.03mM NaCl, 0.17mM KCl, 0.33mM
523 $CaCl_2.2H_2O$, 0.33mM $MgSO_4.7H_2O$). Oxytocin neurons were ablated by treating 5 dpf
524 *Tg(oxt:gal4-VP16; UAS:NTR-mCherry)* larvae on the background of either *Tg(l-fabp:eGFP)*
525 or *Tg(kdrl:eGFP)* with 5uM Nifurpirinol (NFP; LGC, 13411-16-0) for 18h at 28.5^0C in E3
526 media. Larvae where then washed for two hours in E3 media before live imaging. Controls for
527 the experiment were *Tg(oxt:gal4-VP16; UAS:NTR-mCherry)* negative siblings which were
528 also treated with NFP to account for the effects of the drug itself.

529 Oxytocin receptor signaling was attenuated by treating 6 dpf *Tg(l-fabp:eGFP)* or
530 *Tg(kdrl:eGFP)* larvae with 100mM Oxtr antagonist L-368,899 (No.2641, Tocris Bioscience)
531 dissolved in E3 media for 1hour at 28.5^0C followed by live imaging.

532 Tgfβ receptor inhibition was carried out by treating 4 dpf *Tg(l-fabp:eGFP)* or *Tg(kdrl:eGFP)*
533 larvae with 25uM SB431542 (S4317, Sigma-Aldrich) dissolved in DMSO for 48h at 28.5^0C
534 followed by live imaging.

535 To slow down blood flow in the brain/pituitary, 6 dpf *Tg(l-fabp:eGFP)* or *Tg(kdrl:eGFP)*
536 larvae were incubated in a-bungarotoxin for 150 seconds followed by a wash and live imaging.

537 **Optogenetic activation of oxytocin neurons**

538 Adult *Tg(oxt:gal4-VP16)* were crossed with *Tg(l-fabp:eGFP)* or *Tg(kdrl:eGFP)* and the
539 resultant embryos were injected with 40ng/ul of UAS:CoChR-tdTomato (Addgene; plasmid
540 #124233) construct and 40ng/ml of Transposase mRNA at the single-cell stage. Larvae were
541 visually sorted at 5dpf for strong expression of tdTomato in the oxytocin neurons under a
542 fluorescent stereo microscope. Control larvae were siblings that were not injected with the
543 UAS:CoChR-tdTomato construct. All experimental cohorts were grown in an incubator at
544 28.5^0C in the dark.

545 Hypophyseal capillary was imaged under basal conditions, with minimal light activation of the
546 neurons, followed by 10 minutes of rest. Oxytocin neurons were then stimulated for 5 seconds
547 with a 470nm Fiber-coupled LED (ThorLabs Inc,USA) through a fiber optic cannula (400um,

548 0.39NA; ThorLabs) placed near the head of the larvae at 1.5 mW/mm2, followed immediately
549 by live imaging of the hypophyseal capillary only.

550 **Monitoring and analysis of blood flow velocity**

551 Arbitrary line scans with a length of approx. 20 um along the vessel length were obtained at
552 133 Hz in the *Tg(l-fabp:DBP-eGFP)* transgenic line. These line scans were then combined into
553 a multi-frame time-displacement image (kymograph). Two signals were derived from two
554 different points on the displacement axis, and along the time axis. These signals were a
555 representation of the fluctuation in fluorescence intensities across time. Independently, each of
556 these signals gives a measure of the number of red blood cells (RBCs) flowing through the
557 cross-sectional area of the hypophyseal capillary per unit time. On comparing the two signals
558 from each RBC, taken at points x1 and x2, we get the displacement of the RBC within the time
559 frame between t1 and t2. Using these coordinates, the slope of each RBC was computed, and
560 converted to velocity (**Fig. S1C**). The individual RBC velocities in the given kymograph were
561 then plotted as a function of normalized displacement. With an optimal sampling rate of RBCs
562 per second, individual velocities of the RBCs across time were used to obtain a power density
563 spectrum to identify the frequencies at which the flow velocities oscillate. Changes between
564 basal and treated conditions were also depicted as a change in power of particular frequencies
565 or a shift in the frequency itself using a fast Fourier transform (FFT).

566 **Capillary diameter measurements**

567 To measure capillary diameter, line scans were taken perpendicular to vessel length at 133 Hz
568 in the *Tg(kdrl:eGFP)* line. The length of the line was approx. 40um, which covered both ends
569 of arms of the hypophyseal capillary. These line scans were then combined into a multi-frame
570 time-displacement image (kymograph), where each line perpendicular to the x-axis represents
571 a single diameter trace at the corresponding time (**Fig. S1D**). Signals derived from each line
572 corresponding to time values on the x-axis were plotted to obtain two Gaussians each
573 representing the left or right vessel wall. Inner and outer diameter measurements were obtained
574 by measuring the distance between the inner and outer Full-Width Half-Maxima (FWHM)
575 values of these Gaussians. This diameter measured is then converted from pixels to microns
576 and plotted as the final graph as the diameter changes across time for both basal and treated
577 conditions.

578

579 **Vascular permeability assay**

580 Permeability was visualized and quantified using the *Tg(l-fabp:DBP-EGFP)* reporter by
581 employing fluorescence recovery after photobleaching (FRAP) to determine the average
582 recovery half-time ($T_{1/2}$) of the extravasated DBP-EGFP signal. This was carried out by
583 defining two circular regions of interest (ROIs), each of 5µm in diameter, on either side of the
584 hypophyseal capillary. A line scan path (pixel size 0.06um) was drawn perpendicular to
585 direction of flow, through the vessel, and through the centers of the two ROIs. Basal
586 measurements of raw fluorescence were obtained, followed by bleaching the ROI in the area
587 within the hypophyseal loop (**Fig. 6A**). Photobleaching was performed at 100% laser power
588 (approx. 3500mW) for 2.2s at 870nm, followed by the acquisition of the recovery of
589 fluorescence along the line scan path. Raw fluorescence was extracted directly by Zen and was
590 exported to MATLAB to calculate $T_{1/2}$ values. $T_{1/2}$ was calculated by fitting an exponential
591 curve to the recovery florescence and calculating the intercept on the time axis at the point of
592 50% of the maximal fluorescence. The unbleached ROI was used as a control for unintentional
593 bleaching, and basal fluorescence was used to validate the maximal fluorescence values after
594 recovery.

595 **Whole-mount immuno-fluorescence, HCR mRNA in-situ hybridization**

596 Six day-old larvae were fixed in 4% PFA, followed by PBST washes and overnight incubation
597 with 100% Methanol at -20C. Larvae were washed with PBST (0.5% Tween-20 in 1x
598 Phosphate Buffered Saline), incubated in blocking solution for 1 hour at room temperature,
599 followed by overnight incubation at 4C with Guinea Pig anti-oxytocin antibody (Peninsula
600 Laboratories International Inc., CA, USA, no. T-5021) in a blocking solution (5% goat serum
601 in PBST). Larvae were washed with PBST, and then incubated for 4 hours at room temperature
602 with Mouse anti-guinea pig Cy5 secondary antibody (Jackson ImmunoReasearch Laboratories,
603 PA, USA) followed by PBST washes.

604 Hybridization chain reaction (HCR) in-situ v3.0 probes for *c-fos mRNA* were custom designed
605 and synthesized by Molecular Instruments (USA). In-situ hybridization was performed
606 according to Chen et al. (*15*) .

607 Larvae were then mounted in 75% glycerol and imaged with a 40x oil immersion lens using
608 the Zeiss LSM800 confocal setup using the appropriate emission/excitation filters.

609 **FACS Sorting and qRT-PCR**

610 Five adult pituitaries of the *Tg(kdrl:eGFP)* transgenic line were dissected into Ca^{2+} free
611 Ringer's solution (116 mM NaCl, 2.9 mM KCl, 5.0 mM HEPES, pH 7.2), followed by a 30
612 minute incubation in 1X TrypLE Express (Gibco, 12604-013). Pituitaries were then mashed
613 onto a 40um cell stainer and flushed into an Eppendorf using 500ul suspension buffer (L15
614 media without phenol red (Gibco, 21083-027), 1% FBS, 0.5% pen-strep solution). 25ul of
615 20ug/ml DAPI was added, and the cells were sorted into three populations: all pituitary cells
616 (GFP+ and GFP-), endothelial cells only (GFP+), and endothelial depleted (GFP-).
617 populations. Cells were collected in a lysis buffer (0.3% NP-40, 0.1% FBS, 1% RNase
618 Inhibitor) and converted into cDNA directly (Takara, #RR036A). qRT-PCR was performed
619 with 200cells per well and three technical triplicates using the following gene-specific primers:

Gene	Forward Primer (5' -> 3')	Reverse Primer (5' -> 3')
B-actin	TCTTCACTCCCCTTGTTCACAA	TGCCAACCATCACTCCCTGA
kdrl	TCCCCTTACCCTGGCTTACA	GTGGGCCTCTGAGATGGTTC
pdgfrB	TTGTCGAGGCAACAGCGTAT	CTGCGAGCCGTTGATTTGAG
oxtra	TTCTCCGTGCAGATGTGGTC	TAGAGCGTGGAGCAGCAAAA
oxtrb	TACATCATCTGCTGGACGCC	TGCATGAGATCCCGGAACAG

620

621 **Codes**

622 All algorithms to measure velocity, diameter and permeability were custom written on
623 MATLAB (Mathworks, USA) and are available on request.

624 **Statistical analysis**

625 All statistical analyses and graphing were performed using PRISM 10.2 (GraphPad Software
626 Inc, San Diego, USA). Data tables were exported from MATLAB to Prism were required. The
627 normality of the data sets were tested using the Shapiro-Wilk test, and parametric/non-
628 parametric tests were carried out with either a Paired t-test, Mann-Whitney test or the Wilcoxon
629 test for paired samples. All the tests were two-tailed analyses. Welch's ANOVA with Geisser-
630 Greenhouse corrections or Kruskal-Wallis tests was carried out where appropriate with
631 multiple comparisons (Dunnett's, Dunn's or Tukey's). Significance thresholds for all analyses
632 were set at a 0.05 threshold and p-values were corrected for multiple comparisons were
633 necessary. No data points were excluded as outliers in all analyses.

Theoretical resolution of hypophyseal vascular response

Expressing Poiseuille's law for fluid flow through a vessel in terms of flow velocity and vessel radius, we get:

$$V = \frac{r^2 \Delta p}{8\mu L}$$

where r is the radius of the vessel, V is the velocity, Δp is the pressure difference between the two ends of the vessel, μ is the viscosity, and L is the length of the vessel (*54*).

To account for the geometry of the vascular microcircuit, we reduced the hypophyseal vasculature as a function of their vascular resistances (**Fig. 2G**).

$$R_{tot} = R_1 + \frac{R_2^2}{2R_2}$$

$$\text{Total Flow, } Q_{tot} = \frac{\Delta p}{R_{tot}} = \frac{\Delta p}{R_1 + \frac{R_2}{2}}$$

where R_{tot}, R_1, and R_2 are the total resistance, arterial and capillary resistance respectively, and Q_{tot} is the total flow rate.

Pressure difference in the capillary, $\Delta p_2 = Q_{tot} R_{par}$

$$\Delta p_2 = \frac{\Delta p}{R_1 + \frac{R_2}{2}} \cdot \frac{R_2}{2}$$

$$V_2 = \frac{Q_2}{A_2} = \frac{\Delta p}{2R_1 + R_2} \cdot \frac{1}{\pi r_2^2}$$

where R_{par} is the total resistance on the parallel arms of the hypophyseal capillary

Breaking down the denominator and expressing resistance in terms of radius, we get:

$$2R_1 r_2^2 + R_2 r_2^2 = \frac{8\mu}{\pi}\left(\frac{2L_1 r_2^2}{r_1^4} + \frac{L_2}{r_2^2}\right)$$

where r_1 and r_2 are the radii of the artery and capillary, L_1 and L_2 are the lengths of the artery and capillary, respectively.

Substituting the above equation back in the original equation, and L_1 / L_2 = $2.5L_2$ (experimentally derived):

$$V_2 = \frac{r_1^4 r_2^2 \Delta p}{8\mu L_2 (5r_2^4 + r_1^4)}$$

From this equation, given our experimental data, we derived a range of Δp values by pair matching different combinations of mean velocity and radii from out experimental cohorts. A velocity vs radius graph was then plotted using a range of radii with the above pre-defined sets of values for each curve (**Fig. 2H**).

661 **LEGENDS TO FIGURES**

662 **Figure 1. Physiological osmotic challenge increases local hypophyseal blood flow**
663 (**A**) Representative image and scheme showing the hypophyseal neurovascular interface of the
664 transgenic 6-day-old zebrafish larval *Tg(oxt:eGFP;kdrl:mCherry)*. Oxytocin axonal termini
665 and blood vessels are labelled in green and red respectively. (**A, right**) Schema depicting the
666 stereotypic anatomical structure of the hypophyseal artery (HyA), capillary (HyC) and vein
667 (HyV), as well as the anterior mesenchephalic central artery (AMCtA), which was used as a
668 control. Arrows indicate the positions of line scans imaging through and across the vessel were
669 employed to acquire changes in capillary diameter and red blood cell (RBC) velocity traces.
670 (**B**) Scheme showing the production of DBP-eGFP under the liver promoter, L-fabp, in the
671 *Tg(l-fabp:DBP-eGFP)* transgenic line labelling the serum. (**C**) Snap shot of the hypophyseal
672 capillary loop of the *Tg(l-fabp:DBP-eGFP)* transgenic larvae at 6dpf. Dark shadows are
673 created by the red blood cells (RBCs) on a background of DBP-eGFP labelled serum.
674 (**D-E**) Transgenic *Tg(oxt:eGFP)* zebrafish larvae with labeled oxytocin (OXT) neurons were
675 incubated with hyperosmotic solution equivalent to 50% seawater (17.5 ppt) followed by in-
676 situ hybridization of the activity-dependent *c-fos mRNA.* Representative image of a single z-
677 plane (**D**) showing increased *c-fos* expression in OXT neurons following the osmotic challenge
678 quantified (**E**) as the number of *c-fos* positive OXT neurons expressing cells ($p < 0.0001$, Mann-
679 Whitney test, naïve n=9, OC=10). Scale bar, 20um.
680 (**F**) Representative blood flow traces in the HyC at basal conditions and following the osmotic
681 challenge (OC) which led to increased mean RBC velocities in the HyC (**G,** p=0.001, Paired t-
682 test, n=9) and higher variability of velocities measured by spread of individual velocities
683 around the mean (**H,** p=0.0039, Wilcoxon test, n=9). Single-sided amplitude spectra of the
684 velocities (**I**) indicate an increase in amplitudes for frequencies less than 2Hz following the
685 OC.
686 (**J-M**) Osmotic challenge induced no changes to the blood flow traces (**J**), mean velocity (**K**,
687 p=0.2296, Paired t-test, n=7), variability in velocities (**L**, p=0.2669, Paired t-test, n=7), or any
688 changes in the spectra (**M**) in the AMCtA which served as control for the specific effect of the
689 OC.
690

691 **Figure 2. Hypophyseal vascular response is determined by it's geometry.**
692 Changes in capillary diameter in the HyC (**A-C**) and AMCtA (**D-F**).

693 (**A-F**) Representative diameter traces of HyC (**A**) and AMCtA (**D**). Mean diameter of the
694 capillary significantly decreases after OC (**B**, p=0.0156, Wilcoxon test, n=7), as further shown
695 as a ratio of diameter change to basal diameter (**C**, p=0.0006, Mann-Whitney test, n=7).
696 (**D-F**) OC did not affect the mean diameter (**E**, p=0.3076, Paired t-test, n=7), or the ratio of
697 diameter change to basal diameter (**F**, p=0.6900, Mann-Whitney test, n=7) of the AMCtA.
698 (**G**) The predicted relationships between hypophyseal diameter and velocity was theoretically
699 resolved according to Poiseuille's law for viscous fluids by representing the individual
700 components the hypophyseal vascular microcircuit having an inlet-outlet pressure differences
701 (Δp). The corresponding resistance (R), length (L), and radius (r) of the hypophyseal artery
702 (HyA) and capillary (HyC) are indicated. The resulted equation of hypophyseal flow velocity
703 (V_2) as a function of the above parameters is shown (**Fig. 2G,** for details, see '*Methods*'
704 section).
705 (**H**) A range of pressure differences, Δp, was determined by multiple random matches between
706 velocity and radii values that were obtained experimentally. This range was plugged into the
707 resolved V_2 equation resulting three curves indicating the relationship between velocity and
708 radii of the hypophyseal capillary for a given Δp. The measured average velocities before and
709 after osmotic challenge (OC) are indicated by dashed lines (**H**). The point of intersection
710 between the corresponding basal and OC velocities and the curves for a given Δp are indicated
711 by the green and red Xs (**H'**). A corresponding increase in velocity following an OC requires a
712 small increase in pressure and vasoconstriction (solid line) or a large decrease in radius (**H'**,
713 dashed line).
714
715 **Figure 3. Ablation of oxytocin neurons attenuates vascular response to an osmotic**
716 **challenge.**
717 (**A**) Schema representing the transgenic *Tg(oxt:gal4;UAS:NTR-mCherry)* larvae, in which
718 oxytocin neurons express the nitroreductase (NTR) enzyme which reduces the drug nifurpirinol
719 (NFP) into a cytotoxic compound causing specific oxytocinergic cell death.
720 (**B-C**) *Tg(oxt:gal4;UAS:NTR-mCherry)* larvae were treated for 18 hours with 5uM NFP and
721 immune-stained with and antibody directed to endogenous OXT protein. NTR- (control) and
722 NTR+ (Ablated) siblings were treated with NFP, followed by anti-OXT antibody staining.
723 Representative confocal z-stacks images show a reduction of OXT protein in
724 neurohypophyseal axonal projections following NFP treatment of NTR-positive larvae (**B**).
725 Scale bar, 10um. Quantification of OXT-immunoreactive fluorescence shows significantly

726 reduction of OXT in neurohypophyseal termini in the NTR+ cohort (**C**, p<0.0001, Mann-
727 Whitney test, control n=19, treated n=19).
728 Blood flow velocity traces representing the osmotic challenge (OC) increase in hypophyseal
729 blood flow velocity in control (**D**), but not OXT-ablated (**E**) larvae. (**F**) Mean velocity after OC
730 was increased in NTR- larvae (p=0.0046, Paired t-test, n=7), but not in their NTR+ siblings
731 (p=0.0947, Paired t-test, n=7). (**G, H**) Single sided amplitude spectra of the NTR+ cohort show
732 no difference before and after OC as compared to the controls. Variability in velocity was
733 increased after OC in NTR- cohort also (**I**, p=0.0081, Paired t-test, n=7), but not in their NTR+
734 siblings (**I**, p=0.5781, Wilcoxon test, n=7).
735 (**J-K**) Representative diameter traces before and after osmotic challenge showing capillary
736 vasoconstriction of control NTR- larvae (**J**) compared to vasodilation of ablated NTR+ siblings
737 (**K**).
738 **(L)** Following OC, the hypophyseal capillary of NTR- larvae showed a decrease in diameter
739 (p= 0.0156, Wilcoxon test, n=7) while NTR+ larvae showed an increase in diameter (p=0.0045,
740 Paired t-test, n=7). The ratio between diameter change to basal diameter after OC (**M**) was
741 significantly different between the NTR- and NTR+ cohorts (p<0.0001, Dunn's multiple
742 comparison, NTR- n=7, NTR+ n=7).
743 (**N-P**) Mean velocity (p=0.3941, Paired t-test, n=7), variability of velocity (p=0.6983, Paired
744 t-test, n=7) and diameter (p=0.5249, Paired t-test, n=7) of the AMCtA did not change after OC
745 in NTR+ larvae treated with NFP. The control NTR- larvae treated with NFP also did not show
746 any difference in mean velocity (p=0.3095, Paired t-test, n=7), variability of velocity
747 (p=0.5781, Wilcoxon test, n=7) and diameter (p=0.4430, Paired t-test, n=7) in the AMCtA after
748 OC.
749
750 **Figure 4. Hypophyseal blood flow is regulated by oxytocin signaling**
751 (**A, B**) Representative hypophyseal blood flow velocity traces before and after osmotic
752 challenge (OC). Larvae treated with the Oxtr antagonist (Oxtr ant.) L-368,899 show no change
753 in response to OC as compared to their control sibling. Mean velocity (**C**) after OC in the oxtr
754 ant- cohort show an increase (p=0.0033, Paired t-test, n=7), that is not observed in L-368,899
755 antagonist treated siblings (p=0.2509, Paired t-test, n=7).
756 (**D, E**) Single sided amplitude spectra show that while the frequency spectra of a control cohort
757 were affected the OC, larvae treated with the Oxtr antagonist show no difference. Variability
758 in velocities (**F**) was increased following OC (p=0.0213, Paired t-test, n=7), but not in Oxtr
759 antagonist- treated siblings (p=0.7195, Paired t-test test, n=7).

760 (**G, H**) Representative diameter traces showing vasoconstriction following osmotic challenge
761 of control sibling but not in larvae treated with Oxtr antagonist (**I**) No significant change in
762 the mean capillary diameter of the Oxtr antagonist-treated larvae which were subjected to OC
763 (p=0.3892, Paired t-test, n=7) compared to a decrease in diameter in the control cohort
764 (p=0.0001, Paired t-test, n=7).
765 (**J**) The ratio between diameter change to basal diameter after OC showed a significant
766 difference between the control and antagonist-treated cohorts (p=0.0010, Dunn's multiple
767 comparison, Oxtr ant- n=7, Oxtr ant+ n=7).
768 (**K-M**) Mean velocity (p=0.2008, Paired t-test, n=7), variability of velocity (p=0.8040, Paired
769 t-test, n=7) and diameter (p=0.8509, Paired t-test, n=7) of the AMCtA did not change after OC
770 in Oxtr ant+ larvae. The control Oxtr ant- larvae also did not show any difference in mean
771 velocity (p=0.8573, Paired t-test, n=7), variability of velocity (p=0.8533, Paired t-test, n=7)
772 and diameter (p=0.9422, Paired t-test, n=7) in the AMCtA after OC.
773
774 **Figure 5. Optogenetic stimulation of oxytocin neurons increases hypophyseal blood flow**
775 **and is dependent on oxytocin signaling**
776 (**A-B**) Scheme representing the Gal4-UAS system for expression of a blue light- activated
777 channel rhodopsin (*UAS:CoChR-tdTomato*) in oxytocin (OXT) neurons using *Tg*(oxt:Gal)
778 transgenic driver. (**B**) Representative single z-plane confocal image of oxytocin neurons
779 expressing CoChR-tdTomato. Scale bar, 20um.
780 (**C, D**) Representative blood flow velocity traces before and after light stimulation in larvae
781 expressing CoChR show an increase in blood flow velocity as compared to their control sibling.
782 (**E**) Blue light stimulation of CoChR+ larvae led to an increase in mean peak blood flow
783 velocity (p=<0.0001, Paired t-test, n=7). Control CoChR- siblings were not responsive to the
784 light stimulation (p=0.4688, Wilcoxon test, n=7).
785 (**F**) The ratio between velocity change to basal velocity after light stimulation of the CoChR+
786 cohort increased as compared to their CoChR- sibling cohort (p=0.0225, Dunn's multiple
787 comparison, CoChR- n=7, CoChR+ n=7).
788 (**G**) Representative blood flow velocity traces before and after light stimulation in larvae
789 expressing CoChR and treated with the Oxtr antagonist L-368,899 (Oxtr ant.).
790 (**H**) Mean velocity after light stimulation in the CoChR+ Oxtr ant+ larvae show an increase
791 (p=0.0313, Wilcoxon test, n=7), which was also observed in their CoChR+ Oxtr ant- siblings
792 (p=<0.0001, Paired t-test, n=7). (**I**) The ratio between velocity change to basal velocity after
793 light stimulation in the vehicle-treated CoChR+ was significantly larger as compared to their

794 CoChR+ siblings treated with L-368,899 (p=0.0287, Dunn's multiple comparison, Oxtr ant-
795 n=7, Oxtr ant+ n=7).
796 (**J-K**) Representative diameter traces before and after light stimulation in larvae expressing
797 CoChR show an increase in blood flow velocity as compared to their control sibling.
798 (**L-M**) Mean diameter after light stimulation in the CoChR+ larvae show a decrease (p=0.0043,
799 Paired t-test, n=7), that is not observed in their CoChR- siblings (p=0.3349, Paired t-test, n=7).
800 The ratio between diameter change to basal diameter after light stimulation in the CoChR+
801 cohort is lower as compared to their CoChR- sibling cohort (p=0.0047, Dunn's multiple
802 comparison, CoChR- n=7, CoChR+ n=7).
803 (**N**) Representative diameter trace before and after light stimulation in larvae expressing
804 CoChR and treated with the Oxtr antagonist L-368,899.
805 (**O**) Light stimulation of CoChR+ larvae led to a decrease in mean capillary diameter
806 (p=0.0010, Paired t-test, n=7). The capillary diameter of the antagonist-treated CoChR+ larvae
807 did not respond to the optogenetic activation (p=0.6043, Paired t-test, n=7).
808 (**P**) The ratio between diameter change to basal diameter after light stimulation of the
809 antagonist-treated CoChR+ larvae were significantly lower as compared to vehicle-treated
810 CoChR+ sibling cohort (p=0.0060, Dunn's multiple comparison, Oxtr ant- n=7, Oxtr ant+
811 n=7).
812 Dashed lines in all representative traces indicate a LOWESS curve fitted to the data with a
813 smoothing window of ten points.
814
815 **Figure 6. Hypophyseal vascular permeability is regulated by oxytocin signaling**
816 (**A**) Graphical representation of the permeable hypophyseal capillary visualized in the *Tg(l-*
817 *fabp:DBP-eGFP)* larvae. (**A'**) Scheme depicting the hypophyseal capillary permeability assay
818 in which fluorescent recovery after photobleaching (FRAP) of the extravasated DBP-EGFP
819 signal the *Tg(l-fabp:DBP-EGFP)* reporter was measured in a region of interest (ROI) within
820 the hypophyseal capillary loop (red circle) compared to a control ROI outside of the loop. (**B**)
821 A kymograph representing a line scan across time showing the bleached and unbleached ROIs
822 on either side of the hypophyseal capillary, which is marked by dashed lines. The bleaching
823 time point is marked by an arrowhead. (**C**) Average FRAP recovery half-time $T_{1/2}$ was
824 decreased after osmotic challenge (OC) (p<0.0001, Paired t-test, n=8).
825 (**D**) Kymographs representing FRAP traces of naïve (unchallenged) larva displaying vehicle-
826 treated control larva and larva treated with 25 μM of the Tgfβ receptor inhibitor SB431542

827 (TgfβR in.). The bleaching time point is marked by an arrowhead. Higher intensity images of
828 the FRAP kymographs before and after photobleaching are shown on the right (**D'**).
829 (**E**) The basal $T_{1/2}$ values of SB431542-treated larvae were significantly higher than their
830 vehicle-treated siblings ($p<0.0001$, Dunnett's multiple comparison, TgfβR inh.- n=7, TgfβR
831 inh.+ n=7). Larvae treated with SB431542 exhibit a decrease in $T_{1/2}$ values after OC ($p=0.0002$,
832 Paired t-test, n=7) as do their vehicle-treated control larvae ($p=0.0012$, Paired t-test, n=7).
833 (**F**) Mean blood flow velocity values following OC was increased in larvae that were treated
834 with the TgfβR inhibitor ($p<0.0001$, Paired t-test, n=7) as do their vehicle-treated controls
835 ($p=0.0007$, Paired t-test, n=7).
836 (**G**) Representative kymographs of larvae exhibiting basal versus reduced blood flow.
837 (**H**) Application of 1 mg/ml of α-bungarotoxin for 30 seconds immobilizes larvae without
838 affecting blood flow velocity (basal), whereas incubation with α-bungarotoxin for 150 seconds
839 reduced mean blood flow velocity values ($p<0.0001$, Paired t-test, n=13).
840 (**I**) Reduction in blood flow velocity did not affect capillary permeability as indicated by FRAP
841 measurements of $T_{1/2}$ values ($p=0.0854$, Paired t-test, n=13).
842 (**J**) Hypophyseal capillary permeability was monitored at 20 mins intervals before and after the
843 application of Oxtr antagonist. A significant increase in $T_{1/2}$ after 40 and 60 mins of antagonist
844 treatment ($p=0.8090$, Basal *vs*. 20min; $p=0.0004$, Basal vs 40min; $p<0.0001$; Basal *vs*. 60min,
845 Dunnett's multiple comparison, n=7).
846 (**K**) The increment in capillary permeability which is induced by OC ($p<0.0001$, Paired t-test,
847 n=7) is blocked in larvae which were treated with the Oxtr antagonist L-368,899, showing no
848 change in $T_{1/2}$ after OC ($p=0.6147$, Paired t-test, n=7). In accord with Fig. 6J above, basal $T_{1/2}$
849 values of L-368,899- treated larvae were significantly higher than their untreated siblings
850 ($p<0.0001$, Dunnett's multiple comparison, Oxtr ant- n=7, Oxtr ant+ n=7).
851 (**L**) Optogenetic activation of OXT neurons was performed using oxt:Gal;*UAS:CoChR-*
852 *tdTomato* transgenic larvae, as described in the legend to Figure 5 following by FRAP-based
853 permeability measurements. Blue light stimulation of CoChR+ larvae led to a decrease in $T_{1/2}$
854 values ($p=0.0003$, Paired t-test, n=7). $T_{1/2}$ values were unaffected by light in CoChR- larvae
855 ($p=0.2559$, Paired t-test, n=7).
856
857 **Supplemental Fig. S1.**

858 (**A**) Graphical depiction of experimental workflow where either osmotic challenge or
859 optogenetic stimulation is administered to the zebrafish larvae followed by live *in-vivo* awake
860 imaging.
861 (**B**) Kymograph shows red blood cells (RBCs) as black streaks on a background of serum
862 labelled with DBP-eGFP. Signals from each RBC, taken at points x1 and x2, denote the
863 displacement of the RBC within the time frame between t1 and t2. The velocity is given by the
864 tangential derived from these components. (**C**) A kymograph across the blood vessel where
865 each line perpendicular to the x-axis represents a single diameter trace at the corresponding
866 time. $d_1(t)$ and $d_2(t)$ represent the position of the inner walls of the vessel on the displacement
867 axis for a given time, t.
868 (**D**) Diameter of the hypophyseal artery shows no change after OC (p=0.1783, Paired t-test,
869 n=7).
870
871 **Supplemental Fig. S2.**
872 (**A**) Adult pituitary sorted for all cells, endothelia only, and endothelia depleted populations
873 show an enrichment of *oxtrb* mRNA in the endothelial population. *oxtra* mRNA was enriched
874 in the endothelial depleted population but was still observed in low levels in the endothelia
875 population. All comparisons of fold change are made with respect to the mRNA levels of the
876 genes in the entire pituitary.

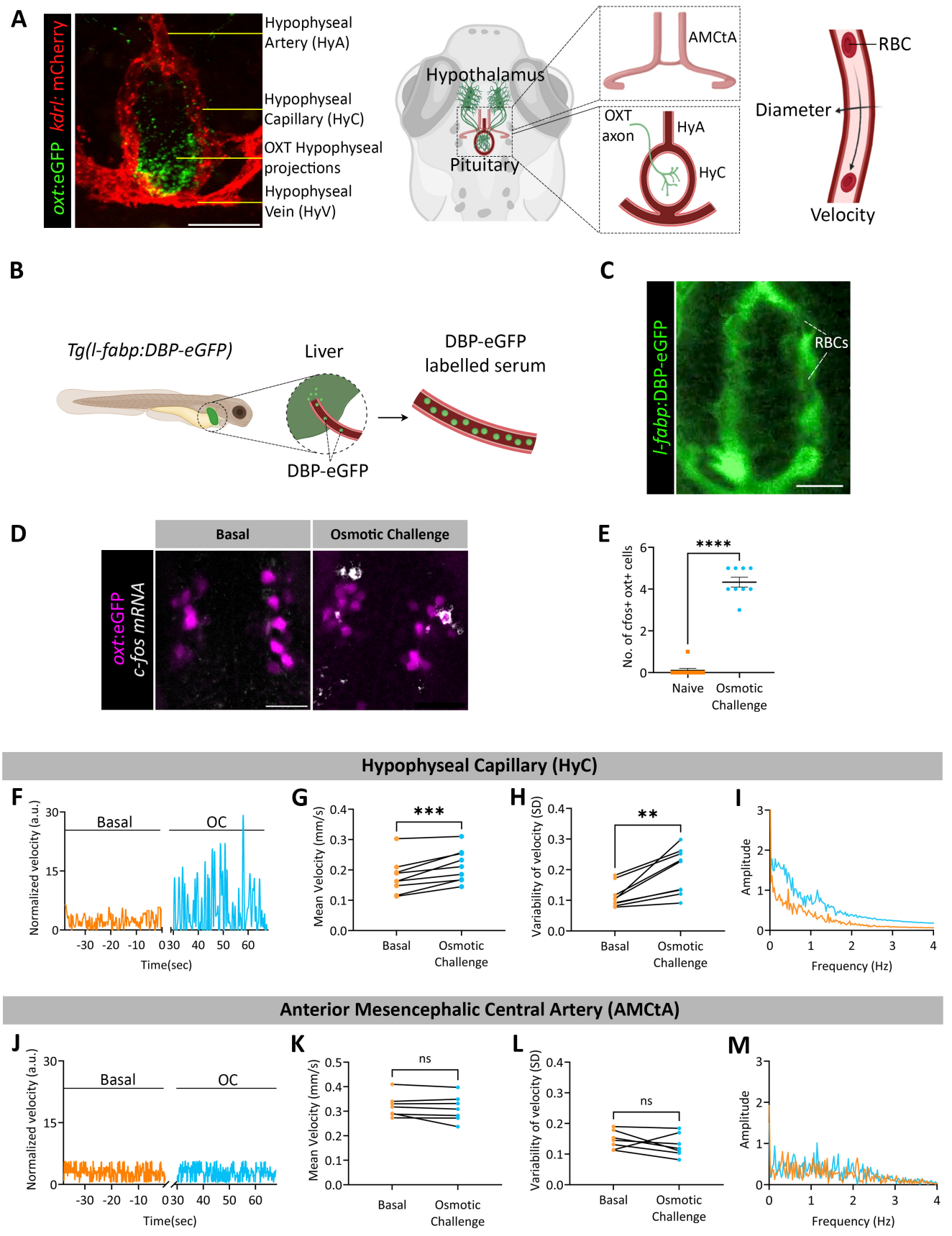
A
oxt:eGFP kdrl: mCherry
Hypophyseal Artery (HyA)
Hypophyseal Capillary (HyC)
OXT Hypophyseal projections
Hypophyseal Vein (HyV)
Hypothalamus
Pituitary
AMCtA
OXT axon
HyA
HyC
RBC
Diameter
Velocity
B
Tg(l-fabp:DBP-eGFP)
Liver
DBP-eGFP labelled serum
DBP-eGFP
C
l-fabp:DBP-eGFP
RBCs
D
Basal
Osmotic Challenge
oxt:eGFP c-fos mRNA
E
No. of cfos+ oxt+ cells
****
Naive
Osmotic Challenge
Hypophyseal Capillary (HyC)
F
Normalized velocity (a.u.)
Basal
OC
Time(sec)
G
Mean Velocity (mm/s)
***
Basal
Osmotic Challenge
H
Variability of velocity (SD)
**
Basal
Osmotic Challenge
I
Amplitude
Frequency (Hz)
Anterior Mesencephalic Central Artery (AMCtA)
J
Normalized velocity (a.u.)
Basal
OC
Time(sec)
K
Mean Velocity (mm/s)
ns
Basal
Osmotic Challenge
L
Variability of velocity (SD)
ns
Basal
Osmotic Challenge
M
Amplitude
Frequency (Hz)

Figure 1

Hypophyseal Capillary (HyC)

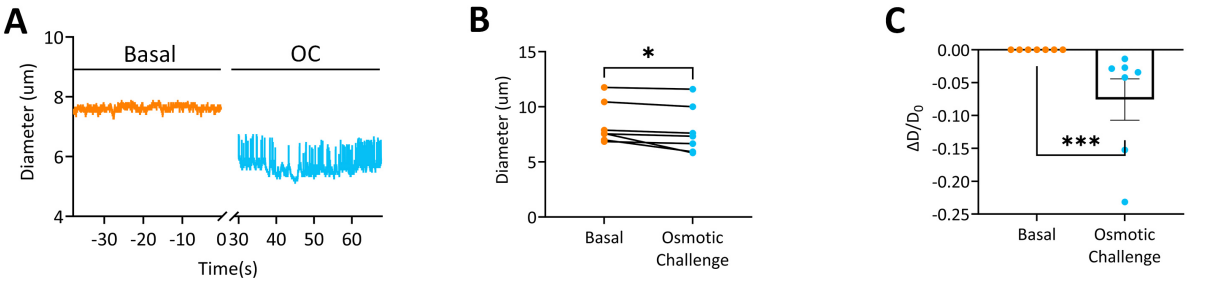

Anterior Mecencephalic Central Artery (AMCtA)

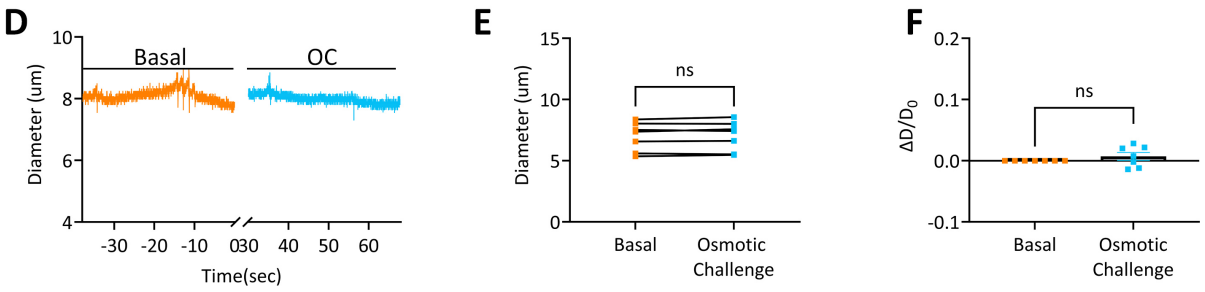

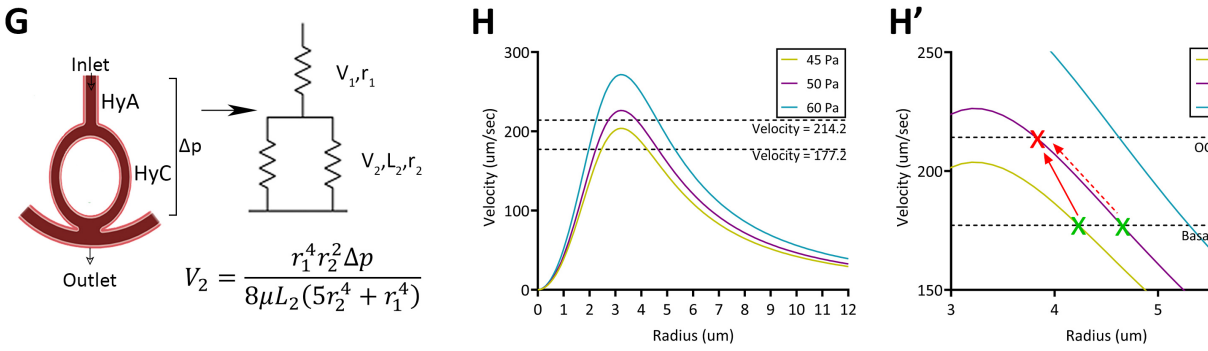

$$V_2 = \frac{r_1^4 r_2^2 \Delta p}{8\mu L_2 (5r_2^4 + r_1^4)}$$

Figure 2

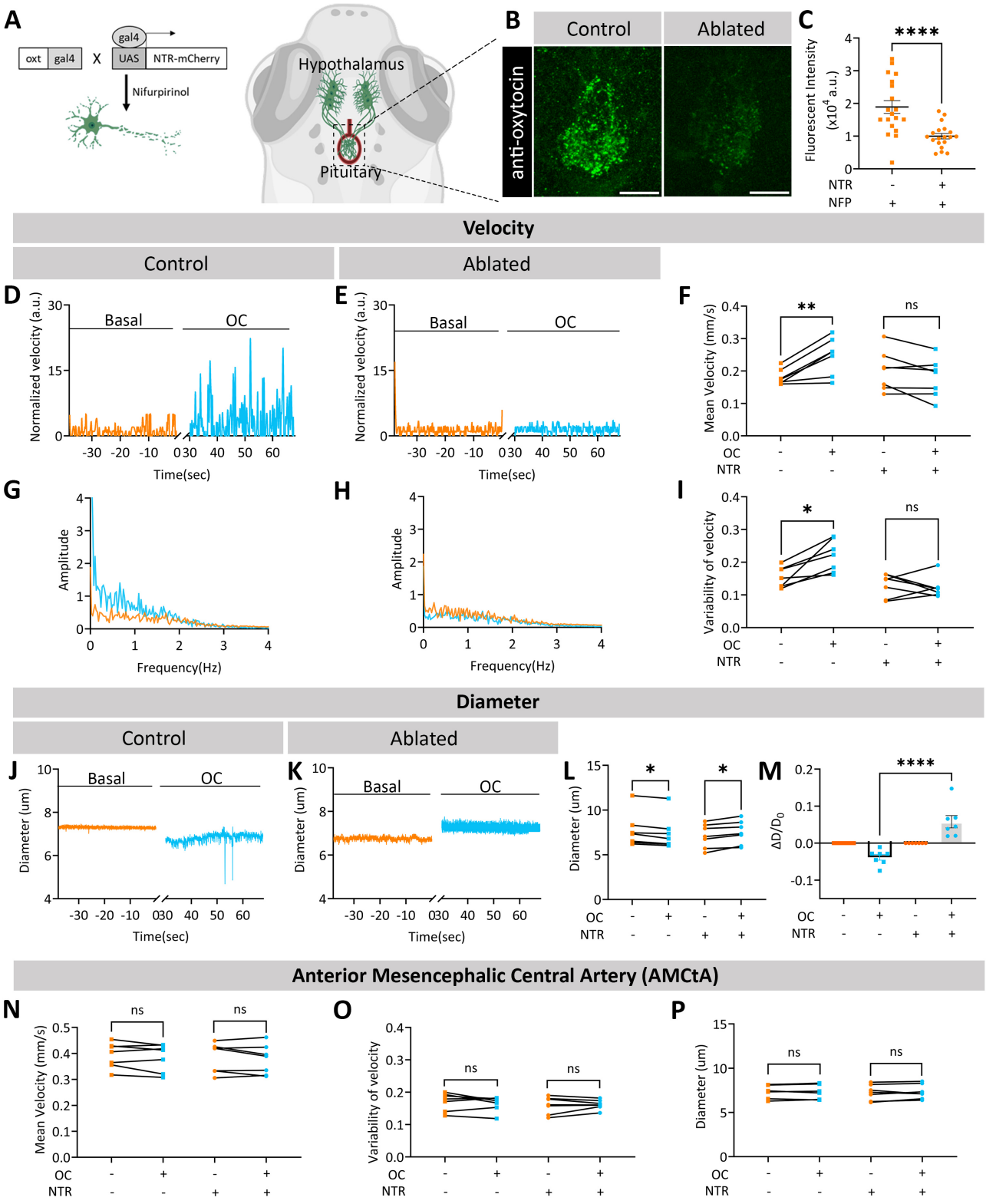
A
oxt
gal4
X
gal4
UAS
NTR-mCherry
Nifurpirinol
Hypothalamus
Pituitary
B
Control
Ablated
anti-oxytocin
C
Fluorescent Intensity (x10^4 a.u.)
****
NTR
NFP
Velocity
Control
Ablated
D
E
Normalized velocity (a.u.)
Basal
OC
Time(sec)
F
Mean Velocity (mm/s)
**
ns
OC
NTR
G
H
Amplitude
Frequency(Hz)
I
Variability of velocity
*
ns
Diameter
J
K
Diameter (um)
L
M
ΔD/D0
****
Anterior Mesencephalic Central Artery (AMCtA)
N
O
P

Figure 3

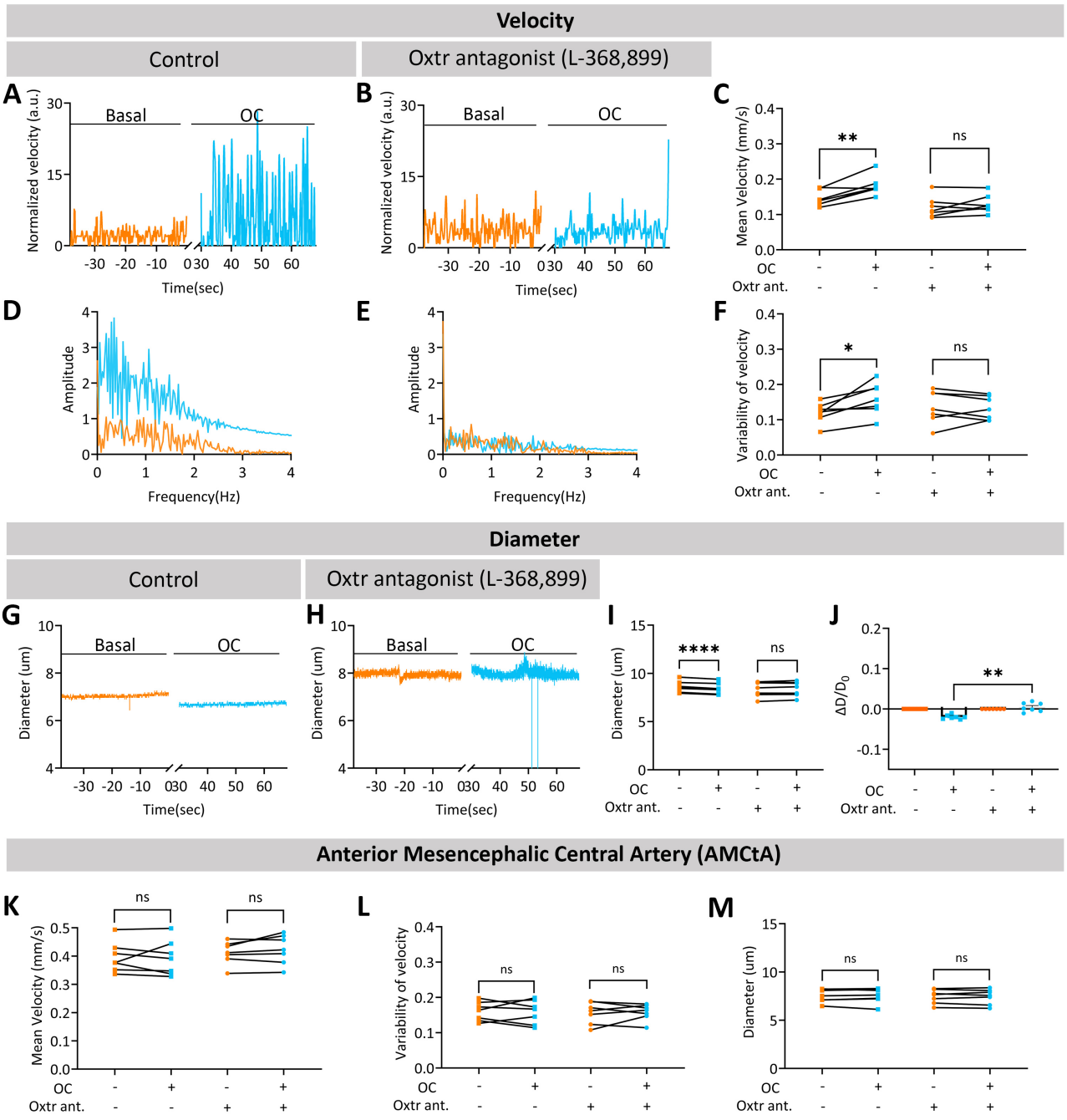
Velocity
Control
Oxtr antagonist (L-368,899)
A
Basal
OC
Normalized velocity (a.u.)
Time(sec)
B
C
Mean Velocity (mm/s)
**
ns
OC
Oxtr ant.
D
Amplitude
Frequency(Hz)
E
F
Variability of velocity
*
Diameter
G
Diameter (um)
H
I
****
J
ΔD/D0
**
Anterior Mesencephalic Central Artery (AMCtA)
K
L
M

Figure 4

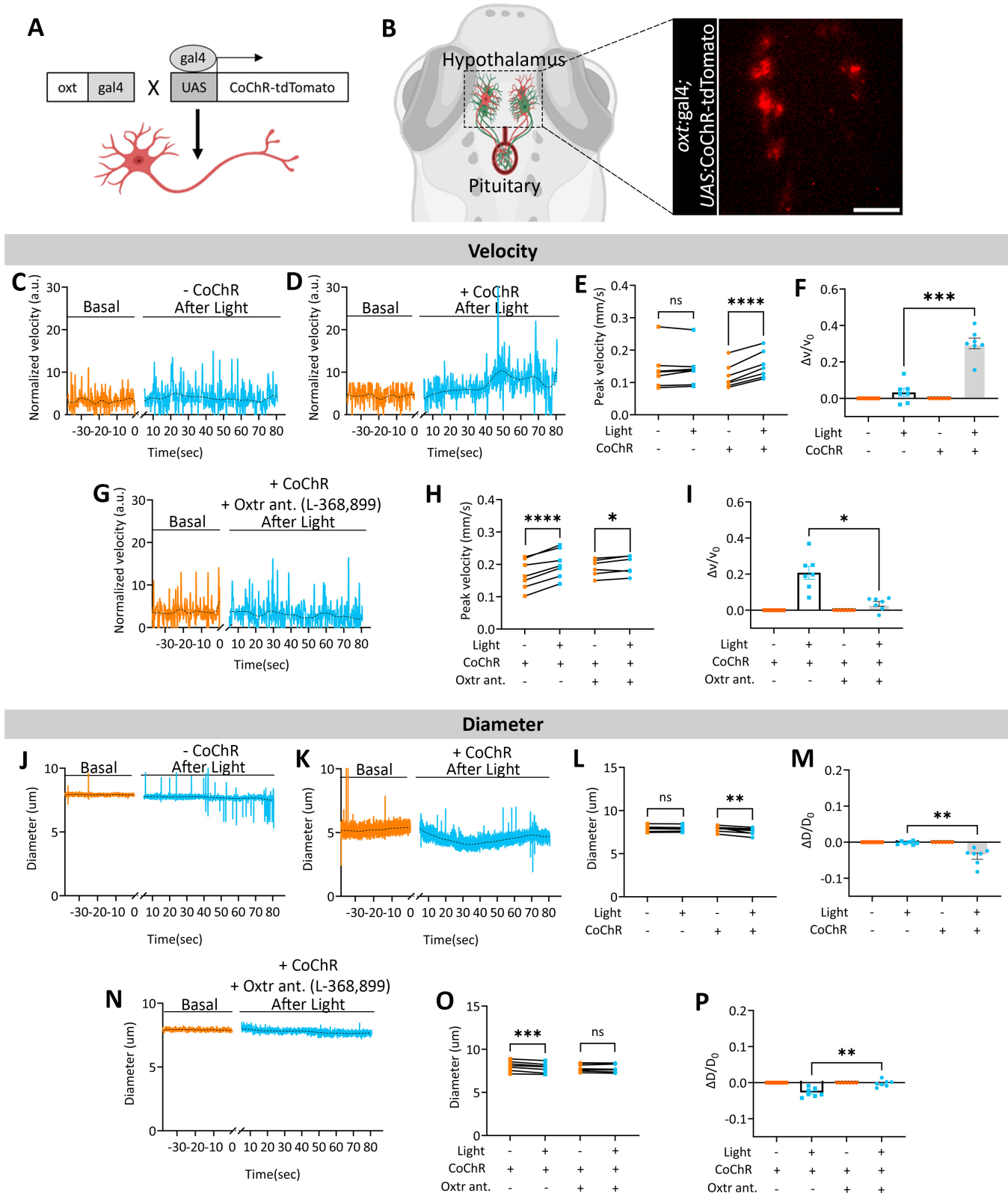
A
gal4
oxt
gal4
X
UAS
CoChR-tdTomato
B
Hypothalamus
Pituitary
oxt:gal4;
UAS:CoChR-tdTomato
Velocity
C
Basal
- CoChR
After Light
Normalized velocity (a.u.)
Time(sec)
D
Basal
+ CoChR
After Light
Normalized velocity (a.u.)
Time(sec)
E
Peak velocity (mm/s)
ns
****
Light
CoChR
F
Δv/v0
***
Light
CoChR
G
Basal
+ CoChR
+ Oxtr ant. (L-368,899)
After Light
Normalized velocity (a.u.)
Time(sec)
H
Peak velocity (mm/s)
****
*
Light
CoChR
Oxtr ant.
I
Δv/v0
*
Light
CoChR
Oxtr ant.
Diameter
J
Basal
- CoChR
After Light
Diameter (um)
Time(sec)
K
Basal
+ CoChR
After Light
Diameter (um)
Time(sec)
L
Diameter (um)
ns
**
Light
CoChR
M
ΔD/D0
**
Light
CoChR
N
Basal
+ CoChR
+ Oxtr ant. (L-368,899)
After Light
Diameter (um)
Time(sec)
O
Diameter (um)
***
ns
Light
CoChR
Oxtr ant.
P
ΔD/D0
**
Light
CoChR
Oxtr ant.

Figure 5

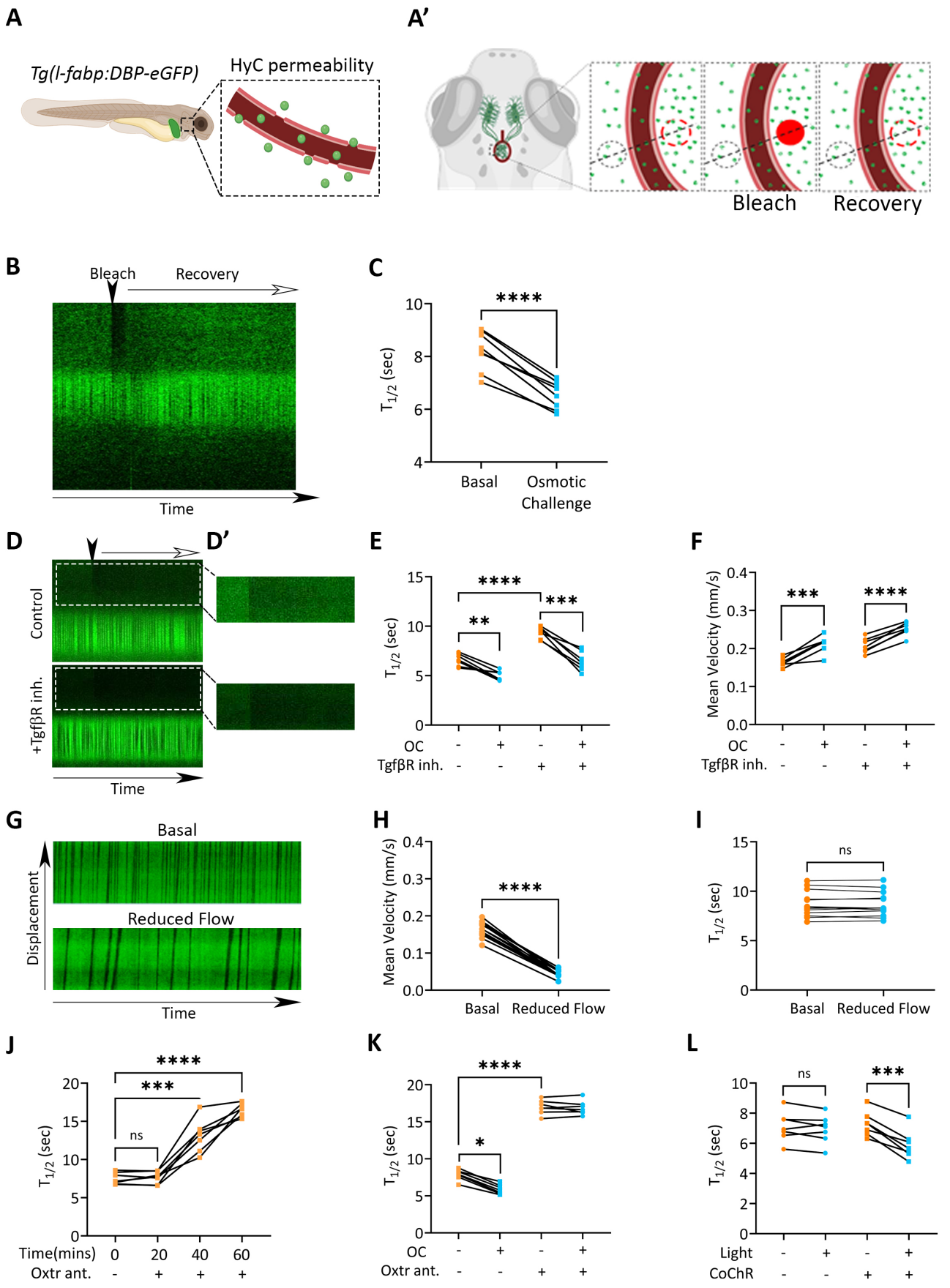
A
Tg(l-fabp:DBP-eGFP)
HyC permeability
A'
Bleach
Recovery
B
Bleach
Recovery
Time
C
****
$T_{1/2}$ (sec)
Basal
Osmotic Challenge
D
D'
Control
+TgfβR inh.
Time
E
****
***
**
$T_{1/2}$ (sec)
OC
TgfβR inh.
F
***
****
Mean Velocity (mm/s)
OC
TgfβR inh.
G
Basal
Reduced Flow
Displacement
Time
H
****
Mean Velocity (mm/s)
Basal
Reduced Flow
I
ns
$T_{1/2}$ (sec)
Basal
Reduced Flow
J
****
***
ns
$T_{1/2}$ (sec)
Time(mins)
Oxtr ant.
K
****
*
$T_{1/2}$ (sec)
OC
Oxtr ant.
L
ns
***
$T_{1/2}$ (sec)
Light
CoChR

Figure 6

A

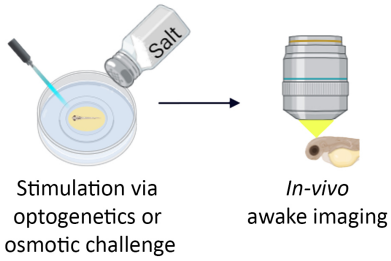

B

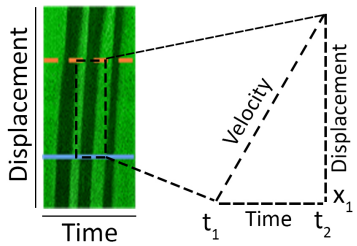

C

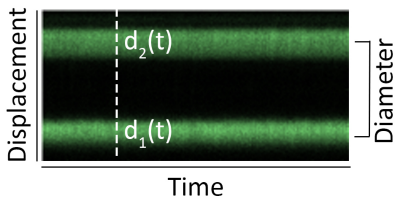

D

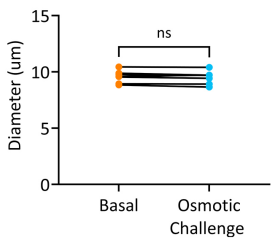

Supplement 1

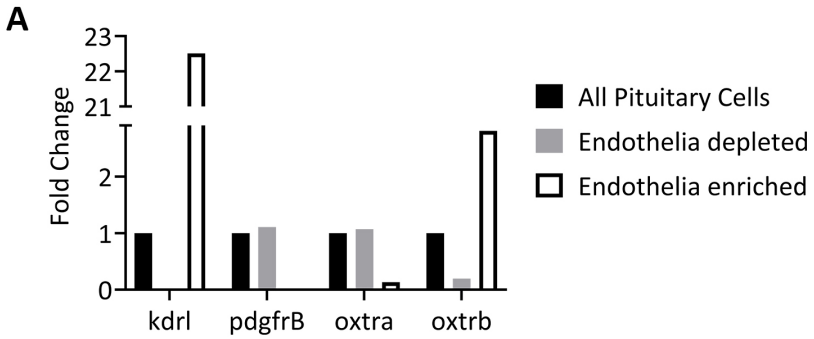

Supplement 2